Microchimica Acta (2022) 189: 2
https://doi.org/10.1007/s00604-021-05117-0

ORIGINAL PAPER

ZnSe nanodisks:Ti_3C_2 MXenes-modified electrode for nucleic acid liquid biopsy with photoelectrochemical strategy

Yuchan Meng[1] · Nana Qin[1] · Xu Hun[1]

Received: 15 August 2021 / Accepted: 20 November 2021 / Published online: 2 December 2021

Abstract

ZnSe nanodisks:Ti_3C_2 MXene complex was prepared for the first time. Based on its remarkable photoelectrochemical performance, combined with the enzyme-free toehold-mediated strand displacement reaction, a photoelectrochemical biosensor for the detection of the non-small-cell cancer biomarker ctDNA KRAS G12D was developed. ZnSe nanodisks were in situ grown on Ti_3C_2 MXene surface by two-step hydrothermal method. The high conductivity and adjustable band gap of MXene significantly enhanced the photoelectric response of ZnSe. Subsequently, the photoelectrochemical biosensor was prepared by combining with the signal amplification function of *p*-aminophenol and the enzyme-free toehold-mediated strand displacement reaction on the modified ITO electrode surface. Under the optimized conditions, the linear detection range is 0.5 ~ 100.0 fM, and the detection limit is 0.2 fM, which realizes the sensitive detection of KRAS G12D. The photoelectrochemical biosensor constructed opens up a new pathway for the preparation of new Mxene-based composite materials and the research of photoelectrochemical biosensor.

Keywords Zinc selenide · Nanodisc · MXene · Non-small-cell lung cancer · Biomarker · ctDNA · Photoelectrochemical

Introduction

As the technical term for transition metal carbides/carbonitrides/nitrides, MXenes are important kinds of layered structure materials. They have the characteristic of metal–carbon and/or nitrogen host layer.[1, 2] The general formula of MXene is $M_{n+1}X_n$, where M is a transition metal (TM, i.e., Sc, Ti, V, Cr, Zr, Hf, Nb, Mo, Ta, and W), X is carbon and/or nitrogen, and *n* is an integer typically between 1 and 3.[3] Ti_3C_2 MXene is one of the most widely used MXenes and has been widely used in various fields. For example, Yang's group synthesized a 2D CdS/2D MXene Schottky heterojunctions via a sequence of electrostatic self-assembly process and solvothermal method, which boosts the photocatalytic activity for hydrogen evolution;[4] Wang' group reported the MXene@Pt colloidal suspension was prepared by reducing Pt cations into metallic Pt, which was used to construct stable and efficient hydrogen evolution reaction electrocatalyst;[5] Zhi's group used MXene and Zn nanosheets as electrodes, to construct an all-component degradable and rechargeable supercapacitor, and the performance of the supercapacitor far exceeded previous reports;[6] In addition, the terminating functional groups on the surface of MXene (such as -O, -F, -OH) can not only have a strong interfacial chemical reaction with the semiconductor, but also provide active sites for the loading of nanomaterials and metal ions, so MXene is widely involved in compounding semiconductor materials to improve the lifetime of photogenerated electrons of semiconductor materials.[7, 8] At the same time, the low toxicity of MXene makes it a prospect in photoelectrochemical biosensors.[9]

II–VI semiconductors are compounds consisting of elements from groups IIB (Zn, Cd, Hg) and VIA (S, Se, Te) of the periodic table. Owing to the special photoelectric properties: wide direct band gap (0–4 eV), large exciton binding energy, and high electro-optic coefficient, II–VI semiconductors are widely used in the fields of photocatalysis and photophone chemistry.[10, 11] Zinc selenide (ZnSe), a non-toxic II–VI semiconductor with a direct band

Yuchan Meng and Nana Qin contributed equally

✉ Xu Hun
hunxuprof@outlook.com

[1] Key Laboratory of Optic-electric Sensing and Analytical Chemistry for Life Science, Qingdao University of Science and Technology, 266042 Qingdao, People's Republic of China

gap of ~ 2.67 eV, is also widely used due to its huge photoelectric properties and suitable band positions. However, the special defects of ZnSe pure semiconductors are the fast photogenerated carrier recombination rate and narrow spectral response range.[12] Therefore, finding a suitable material to build a heterostructure has been proved to be an effective method to solve this problem, because it has obvious advantages in elevating the charge transfer process and introducing a second semiconductor to broaden the spectral response range.[13].

Liquid biopsy is a method for noninvasive analysis of tumor-associated material in body fluids (blood, saliva, urine, ascites).[14] Circulating tumor DNA (ctDNA) fragments are mainly derived from apoptotic tumor cells, which release their DNA fragments into body fluids. As a new biomarker, ctDNA has a wide application prospect in liquid biopsy due to its simple sampling operation and low price. [15, 16] The current detection of ctDNA mainly focuses on polymerase chain reaction (PCR) technology, such as reverse transcription quantitative PCR (RT-qPCR), asymmetric PCR, and droplet digital PCR (ddPCR).[17] All of these analytical techniques require the efficient catalysis of enzymes to improve their sensitivity. However, the control of the reaction conditions of enzyme activity and the nonspecific and false positive signals it cause make it more challenging.[18] Toehold-mediated strand displacement reaction can amplify detection signal without the involvement of enzymes, which is simple in design and easy to operate, so it is widely used in the construction of biosensors. [19] As a member of the small GTP-binding protein family, RAS proteins play a leading role in regulating cellular responses such as proliferation, differentiation, migration, and cell growth and its abnormal signaling plays a role in up to 30% of human cancers. KRAS, a member of the RAS family, is the most common mutant member of all cancer subtypes, mainly in pancreatic cancer (~ 98%) and colorectal cancer (~ 45%), and its mutation results in glycine-aspartate codon replacement 12 (G12D) or 13 (G13D). KRAS G12D is common in pancreatic cancer and is one of the most important chemotherapy drug targets.[20, 21].

In this study, a solvothermal in situ growth method was used to successfully synthesize ZnSe nanodisks:Ti_3C_2 MXene (ZnSeNDs:Ti_3C_2) with excellent photoelectric properties. Due to the strong chemical reaction between the surface active groups of Ti_3C_2 and the ZnSe interface, the smooth surface of the multilayer Ti_3C_2 is loaded with a large number of disc-shaped ZnSeNDs. Benefiting from the metal conductivity and carrier transport efficiency of Ti_3C_2, ZnSeNDs:Ti_3C_2 has higher carrier separation rate and wider light absorption than ZnSeNDs. A non-small-cell lung cancer biomarker, ctDNA KARS G12D, is selected as the model target nucleic acid.[22] Based on ZnSeNDs:Ti_3C_2 excellent photoelectrochemistry (PEC) properties, combined with strand displacement amplification, a PEC sensor was constructed for detecting KARS G12D.

Experimental

Reagents

Ti_3AlC_2 MAX was ordered from Sciclubs (Zhejiang, China). Zinc nitrate hexahydrate ($ZnNO_3 \cdot 6H_2O$), selenium (Se) power, and hydrofluoric acid (HF, 40%) were pursed from Sinopharm Chemical Reagent Co., Ltd (Shanghai, China). *p*-aminophenylphosphate·monosodium (*p*-APP) was provided by LKT Laboratories Inc. (MN, USA). Streptavidin-labeled alkaline phosphatase (SA-ALP) was bought from Sigma-Aldrich Co., LLC (USA). N,N-Dimethylformamide (DMF) and *p*-aminophenol (*p*-AP) were obtained from J&K Chemical Ltd. (Shanghai, China). 0.1 M pH 7.4 phosphate buffer was consisted of 0.1 M NaH_2PO_4, 0.1 M Na_2HPO_4, and 0.1 mM KCl which was used for PEC measurement. Chitosan (CS) and glutaraldehyde (Glu) solution (50 wt% in H_2O) were provided by Aladdin (Shanghai, China). The KARS G12D, amino-modified template probe (NH_2-TP), assistant probe (AP), Biotin-Fuel strand (Biotin-FS), and protection probe (PP) were synthesized by Sangon Biotech Co., Ltd. (Shanghai, China), and the sequences are provided in supporting information Table S1.

Apparatus

The scanning electron microscopy (SEM) and elemental mapping were recorded on Regulus 8100 scanning electron microscope (Hitachi Ltd, Japan). X-ray diffraction (XRD) was obtained using a 18KW D/MAX/2500PC (Rigaku. Ltd, Japan). The UV–vis and UV–vis DRS was measurement by a Cary Ultraviolet visible spectrophotometer (Agilent Technologies, Inc. USA). PEC and electrochemical measurements were all performed on a CHI660D electrochemical workstation which contained a conventional three-electrode system (Shanghai Chenhua Instrument Co. Ltd., China).

Preparation of multilayered Ti_3C_2

Ti_3C_2 MXene was prepared through etching Al layers from Ti_3AlC_2 MAX following the previous reported literature. [23] Briefly, 1 g Ti_3AlC_2 was added to 40 mL 40% HF solutions, and then reacted at room temperature for 24 h under stirring. Finally, the suspension was centrifuged at 4000 rpm with deionized water for several times until the pH of supernatant over 5. The multilayered Ti_3C_2 was obtained.

Scheme 1 Strategy of *p*-AP oxidation amplification and toehold-mediated strand displacement reaction for *KARS G12D* liquid biopsy using ZnSeNDs:Ti_3C_2 as photoelectric materials

Synthesis of ZnSeNDs:Ti_3C_2

ZnSeNDs:Ti_3C_2 was synthesized with a solvothermal method (Scheme 1a).[24] Firstly, 0.158 g Ti_3C_2 was added in the mixture of ethylenediamine and deionized water solution ($V_{ethylenediamine}$:V_{water} = 2:1, 60 mL), agitating. Then Se powder (0.158 g), $ZnNO_3{\cdot}6H_2O$ (0.595 g), and $NaBH_4$ (0.984 g) were added into the mixture of Ti_3C_2-ethylenediamine-deionized water solution. Then it was transferred to Teflon-lined autoclave (80 mL). It was heated for 12 h at 180 °C. The precipitate was washed with distilled water three times, and the gray precursor was collected. Secondly, $NaBH_4$ (0.984 g), the precursor, and deionized water (15 mL) were added to Teflon-lined autoclave and reacted at 140 °C for 12 h. The precipitate was washed with deionized water and absolute ethanol, and then dried. ZnSe nanodisks (ZnSeNDs) were synthesized by the same method but Ti_3C_2 was not added during preparation of the precursor.

Preparation of ZnSeNDs:Ti_3C_2-modified ITO

Firstly, the indium tin oxide (ITO) electrodes were cleaned with deionized water, ethanol, and deionized water for 5 min, respectively. Then 10 mg ZnSeNDs:Ti_3C_2 was added to 5 mL DMF with 10 min ultrasound to get homogenous suspension. Finally, 2-mg/mL suspension was dropped onto ITO surface to obtain the ZnSeNDs:Ti_3C_2/ITO and dried naturally in the air.

Electrochemical and PEC measurements

PEC response and cyclic voltammetry (CV) of ZnSeNDs:Ti_3C_2/ITO were measured using ITO electrode

as the working electrode, a Pt wire as the counter electrode and a saturated calomel electrode as the reference electrode. 100 mV s^{-1} scan rate was used. Electrochemical impedance spectroscopy was detected in 5.0 mM $[Fe(CN)_6]^{3-/4-}$ with 0.1 M KCl.

Fabrication of biosensor

Because CS has good biocompatibility and film-forming properties, Glu usually acts as a linking molecule to bind both CS and bioactive substance. Therefore, both CS and Glu are often used in the construction of biosensors.[25, 26] CS solution (1% mass fraction) was prepared through dispersing CS powder in 1% acetic acid and Glu was diluted with deionized water to a mass fraction of 5%. First, 10 μL 1% CS solution was added to the surface of ZnSeNDs:Ti_3C_2/ITO drying at 50 °C for 30 min. After washing with 0.1 M NaOH and deionized water, the CS/ZnSeNDs:Ti_3C_2/ITO was obtained. Then 5% Glu was added to the surface of CS/ZnSeNDs:Ti_3C_2/ITO and reacted at 40 °C for 1 h. After washing away the excessive Glu with deionized water, 10 μL double probes were dropped to the modified electrode to react 2 h at 4 °C. The double probes were obtained by heating a mixed solution of three strands (30 μL 3.3 μM NH_2-TP, 30 μL 3.3 μM AP, 30 μL 3.3 μM PP) to 85 °C for 10 min and then slowly cooling to room temperature.

Detection of KARS G12D

After washing the unreacted double probes on the surface of the modified electrode, the double probes/CS/ZnSeNDs:Ti_3C_2/ITO were incubated with 10 μL 10 mM Tris–HCl buffer containing various concentrations of the KARS G12D and 10 μL 1 μM Biotin-FS for 2 h. After washing with 10 mM Tris–HCl buffer, the electrode was used for PEC measurement.

Results and discussion

Characterizations of the prepared materials

In order to explore the morphology of Ti_3AlC_2, Ti_3C_2, ZnSeNDs, and ZnSeNDs:Ti_3C_2, the SEM images were measured. The raw Ti_3AlC_2 presents irregular bulk morphology (Fig. 1A). Figure 1B shows that Ti_3C_2 exhibits multi-layer structures with a smooth surface which is attributed to the disappearance of the Al layer after HF etching. Figure 1C shows that ZnSeNDs has approximate hexagonal disk morphology, and the size is about 80–110 nm. Due to large surface area of Ti_3C_2, a large amounts of ZnSeNDs are located on the surface of Ti_3C_2 (Fig. 1D). Elemental characterizations of ZnSeNDs:Ti_3C_2 were also measured. As shown in Fig. 1E, it suggests the Ti, C, Se, and Zn elements of ZnSeNDs:Ti_3C_2 are homogeneous and continuously distributed.

To further identify the composition and crystal structure of photoelectroactive materials, the XRD was also measured (Fig. 1F). It indicates that the diffraction peaks at 9.5°, 19.06°, 38.7°, and 41.84°are matched well with the diffraction peaks of the standard card (JCPDS card no. 52–0875) of Ti_3AlC_2 (curve a). The disappearance of the diffraction angle corresponding to (104) plane of Al at 38.7° and the diffraction angle corresponding to (002) plane of Ti_3C_2 shifts from 9.5° to 8.27°, indicating the successful preparation of Ti_3C_2 (curve b).[27–29] The diffraction peaks of ZnSeNDs (curve c) appear at 27.2°, 45°, 53.7°, 66°, 72.6°, and 83.5° are matched well with the standard card (JCPDS card no. 37–1463). When ZnSeNDs is grown on the surface of Ti_3C_2, ZnSeNDs:Ti_3C_2 has the characteristic peak of both Ti_3C_2 and ZnSe (curve d), demonstrating that the crystal form has not changed after the combination of ZnSe and Ti_3C_2.[27] The SEM images, mapping, and XRD show that the ZnSeNDs:Ti_3C_2 is successfully synthesized.

Electrochemical and optical properties of the ZnSeNDs:Ti_3C_2-modified ITO electrode

EIS (Fig. 2A) shows that the Ret of ZnSeNDs:Ti_3C_2 significantly decreases compared with the ZnSeNDs, which may attributed to the high charge carrier mobility of Ti_3C_2 suppress the recombination of electron and holes in ZnSeNDs/ITO interfaces. [1, 30, 31] Then the open circuit potential (OCP) test was performed under dark and illuminated conditions to better understand the charge separation process of photoelectroactive materials. As shown in Fig. 2B, under illumination, photopotential of ZnSeNDs:Ti_3C_2 is much larger compared to Ti_3C_2 and ZnSeNDs, suggesting that ZnSeNDs:Ti_3C_2 possesses more driving force for transportation of carriers compared to others.[32] In order to prove the carrier transfer type of the photoelectroactive materials, the Mott-Schottky curve measurement [5, 6] was carried out. According to Eq. 1.

$$\frac{1}{C^2} = \frac{2}{N_D e \varepsilon_0 \varepsilon}\left[\left(E_{S-}E_{FB}\right) - \frac{kT}{e}\right] \quad (1)$$

where

N_D is the donor density;
ε_0 is the permittivity of a vacuum;
ε is the dielectric constant of the material ($\varepsilon = 1.3556$);
E_S is the applied potential;
E_{FB} is the flat band potential; and.
kT/e is the temperature-dependent term.

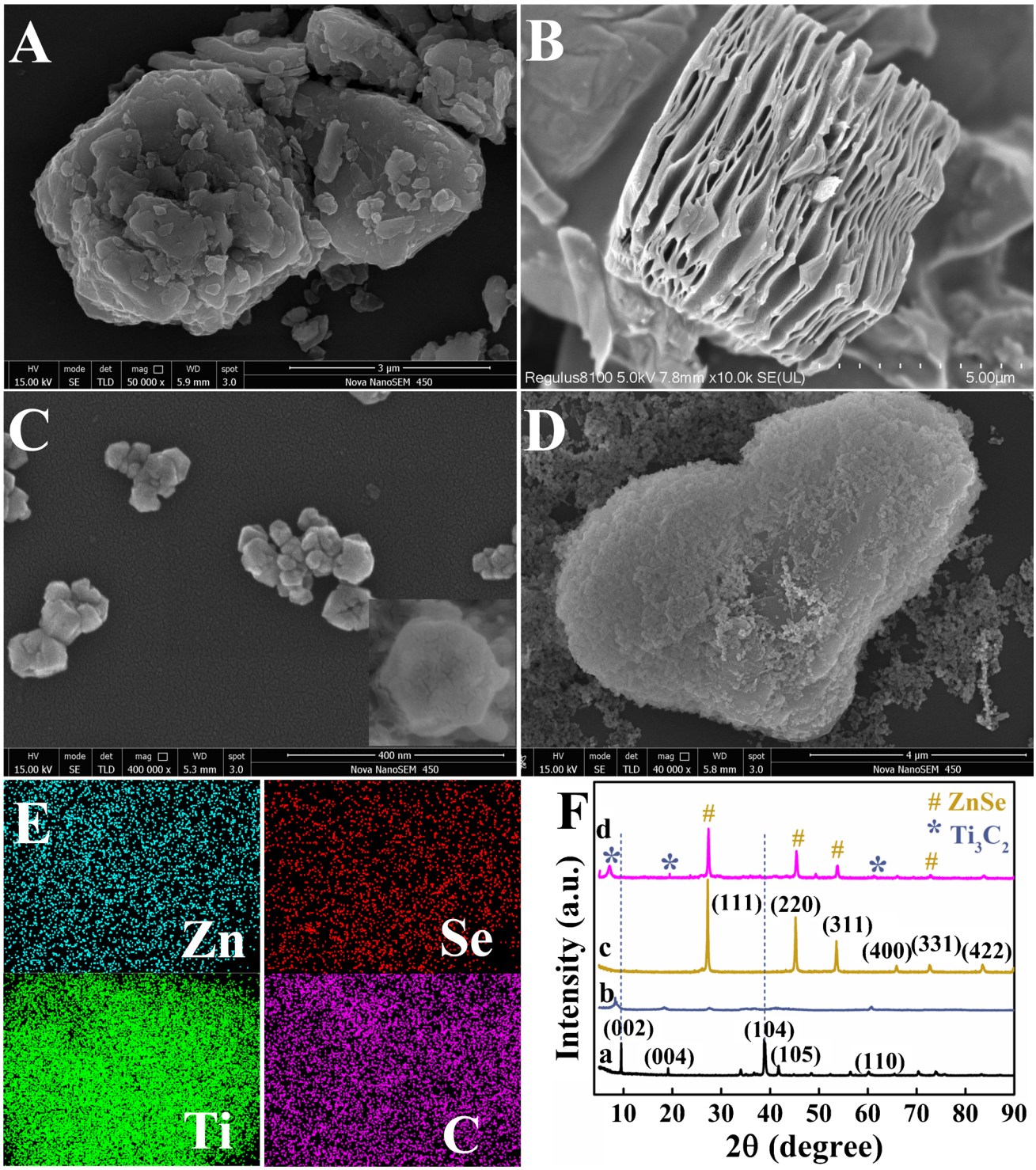

Fig. 1 SEM images of Ti_3AlC_2 (**A**), Ti_3C_2 (**B**), ZnSeNDs (**C**), and ZnSeNDs:Ti_3C_2 (**D**). Elemental mapping images of ZnSeNDs:Ti_3C_2 (**E**). (**F**) XRD of Ti_3AlC_2 (a), Ti_3C_2 (b), ZnSeNDs (c), and ZnSeNDs:Ti_3C_2 (d). The inset in panel (**C**) is a magnification of a ZnSeND

The slope of the linear part of Mott-Schottky plot reflects semiconductor feature and carrier concentration.[33] As shown in Fig. 2C, the slopes of ZnSeNDs, Ti_3C_2, and ZnSeNDs:Ti_3C_2 are all positive, indicating that they show n-type behavior with electrons as the major carriers. In addition, the ZnSeNDs:Ti_3C_2 exhibits a smaller slope, which means that ZnSeNDs:Ti_3C_2 has a greater carrier density. The increase of carrier density in ZnSeNDs:Ti_3C_2 is considered

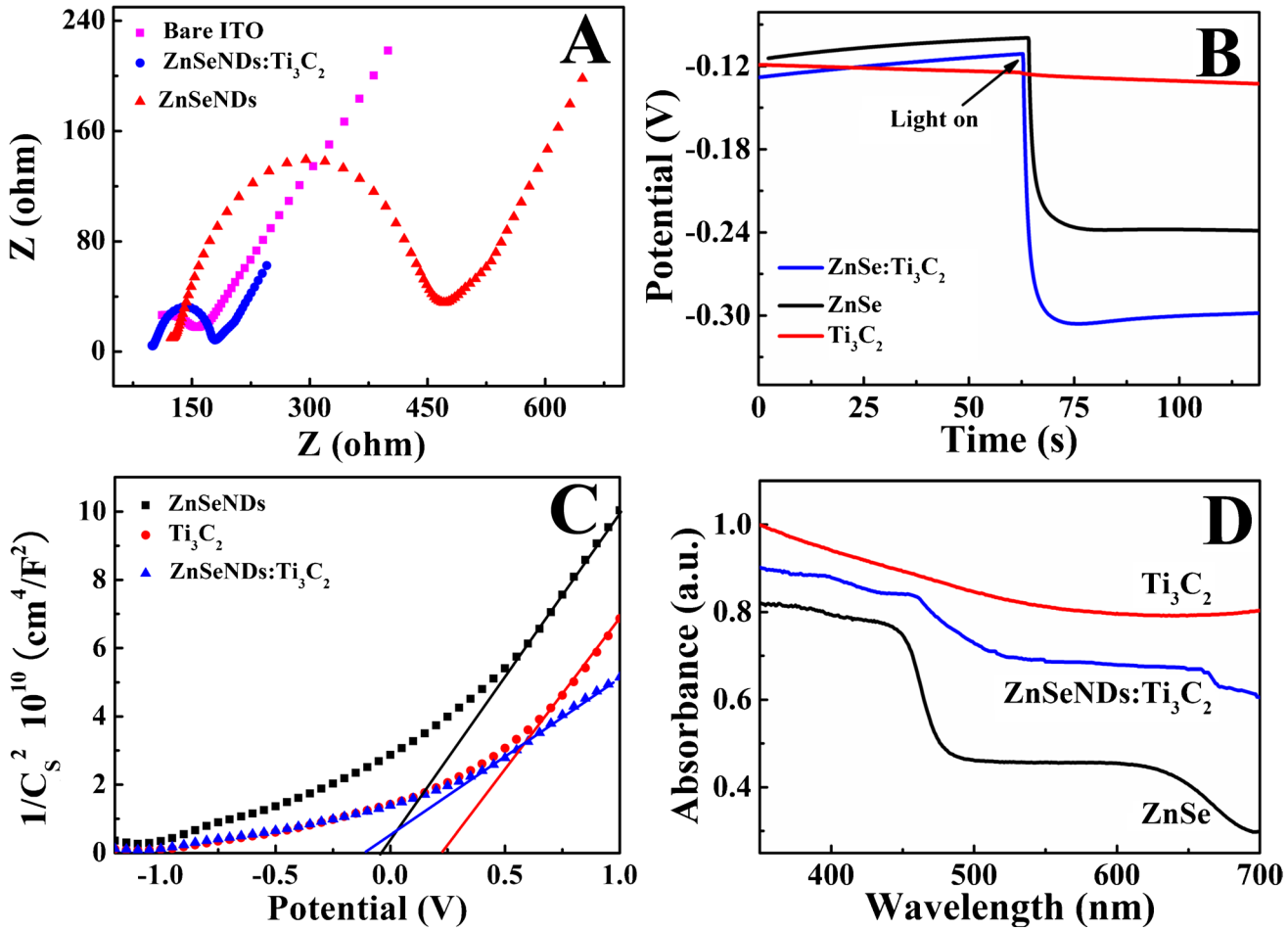

Fig. 2 **A** The EIS response of bare ITO, ZnSeNDs/ITO, and ZnSeNDs:Ti_3C_2/ITO in 5.0 mM $[Fe(CN)_6]^{3-/4-}$ containing 0.1 M KCl. **B** Open-circuit potential response of Ti_3C_2/ITO, ZnSeNDs/ITO, and ZnSeNDs:Ti_3C_2/ITO under dark and illuminated conditions (10 W LED lamp). **C** Mott-Schottky plots of Ti_3C_2, ZnSeNDs, and ZnSeNDs:Ti_3C_2. **D** UV–vis DRS spectra of Ti_3C_2, ZnSeNDs, and ZnSeNDs:Ti_3C_2

to be the main factor for the significant increase of photocurrent density. It is consistent with the phenomenon of OCP. The light absorption behavior of photoelectroactive material deeply impacts on its photoelectrochemical performances. The UV–vis DRS (Fig. 2D) shows that the characteristic absorption edge of ZnSeNDs falls at about 470 nm, which is consistent with previous studies.[34] For ZnSeNDs:Ti_3C_2, as expected, the absorption is remarkably enhanced in the UV–vis region compared with ZnSeNDs. The enhanced visible light absorption demonstrates that it can produce more photogenerated charges in the visible light region.[35].

p-AP redox enhances PEC signal

In order to explore the PEC properties of the Ti_3C_2, ZnSeNDs, and ZnSeNDs:Ti_3C_2, the measurement of *i*–*t* curve was first performed in 0.1 M phosphate buffer (pH 7.4) with and without 1.0 mM *p*-AP. Figure S2A shows that without *p*-AP, the photocurrents of Ti_3C_2, ZnSeNDs, and ZnSeNDs:Ti_3C_2 are about 0.6 μA, 2.8 μA, and 5.6 μA under the optimal potential (Fig. S1), respectively. The combination of ZnSeNDs and Ti_3C_2 realizes the enhancement of PEC response, which may be caused by the high charge carrier mobility of Ti_3C_2. While with the introduction of *p*-AP, the photocurrent signal increases significantly, and the photocurrent of ZnSeNDs:Ti_3C_2 reaches its maximum about 16.1 μA, which is 2.87 folds than that without *p*-AP. As an electron donor, *p*-AP can provide electrons for n-type semiconductor, thus realizing the increase of PEC signal.[36] Subsequently, in order to prove that the participation of *p*-AP leads to the enhancement of PEC response, UV–vis of *p*-AP before and after PEC detection was measured. With the increase of illumination time (0 min, 30 min, 60 min, 90 min, 120 min), the absorption peak intensity of *p*-AP at 292 nm decreases gradually, while in the dark conditions, there is little change in *p*-AP peak intensity (120 min) (Fig. S2B). This shows that

under light conditions, the photogenerated holes promote the oxidation of *p*-AP,[37] and the electrons of *p*-AP are injected into the photogenerated holes to enhance the intensity of the photocurrent.

The PEC mechanism of *p*-AP oxidation amplification strategy

The band gap structure of the material was investigated. The band gap was characterized by Tauc plot which shows that the optical absorption strength depends on the difference between the photon energy and the band gap:[38, 39]

$$(\alpha h\nu)^{1/n} = A(h\nu - E_g) \quad (2)$$

where

ν is the frequency of light;
A is a constant;
h is the Planck's constant;
E_g is the energy band gap of the material;
$n = 1/2$ for direct semiconductor, and $n = 2$ for indirect semiconductor.

ZnSe is a typical direct semiconductor; therefore, the $n = 1/2$.[34] As shown in Fig. 3A, the band gap of the ZnSeNDs is 2.62 eV by extrapolating a straight line along the horizontal axis. According to the intercept of the tangent of the Mott-Schottky curves on the *x*-axis, the derived values of flat-band potentials of ZnSeNDs and Ti_3C_2 are about − 0.043 V vs Ag/AgCl and 0.228 V vs Ag/AgCl (Fig. 2C). For n-type semiconductors, the flat-band potentials are close to the Fermi energy level,[40] as a result, E_{FB} of ZnSeNDs and Ti_3C_2 are close to − 0.043 V and 0.228 V vs Ag/AgCl. On the basis of the above experimental results, the mechanism of *p*-AP oxidation to enhance PEC signal may be shown in Fig. 3B. As the ZnSeNDs:Ti_3C_2 is irradiated with visible-light, the photogenerated electrons (e^-) from the VB of ZnSeNDs are excited to their respective CB, while leaving the photogenerated holes (h^+) behind in VB. Since the Fermi energy level of Ti_3C_2 MXenes is lower than that of ZnSeNDs, electrons from the ZnSeNDs conduction band (CB) are transferred to Ti_3C_2. After the photogenerated electrons are transferred to Ti_3C_2, due to the excellent metal conductivity, they are further rapidly shuttled to ITO electrode. At the same time, the photogenerated holes promote the oxidation of *p*-AP to *p*-quinonimine (*p*-QI), which allows more effective separation and longer lifetime of electron–hole pairs in ZnSeNDs, eventually resulting in the enhanced anodic photocurrent.

The construction of PEC biosensor based on *p*-AP oxidation amplification strategy and ZnSeNDs:Ti_3C_2-modified ITO electrode

Toehold-mediated strand displacement reaction can occur without the helping of enzymes, which has applied in developing different biosensor.[41–43] In toehold-mediated strand displacement reaction, one oligonucleotide binds to the dangling toehold domain of a dsDNA, and triggers a branch migration step, resulting in the dissociation of the strand previously hybridized in the substrate with partial complementarity.[44, 45] Therefore, in this work, we designed two simple toe-mediated chain displacement reactions (Scheme 1b). The KARS G12D was hybridized with the probe to initiate the first toe-mediated chain displacement response, followed by the introduction of Bio-FS to initiate the second toe-mediated chain displacement response while achieving the KARS G12D recycling. Scheme 1 shows the construction of PEC biosensor based on *p*-AP oxidation amplification strategy. First, the surface of the electrode is modified with a layer of CS and Glu to make the electrode surface functionalized. Then the toehold association of strand displacement reaction is achieved by connecting

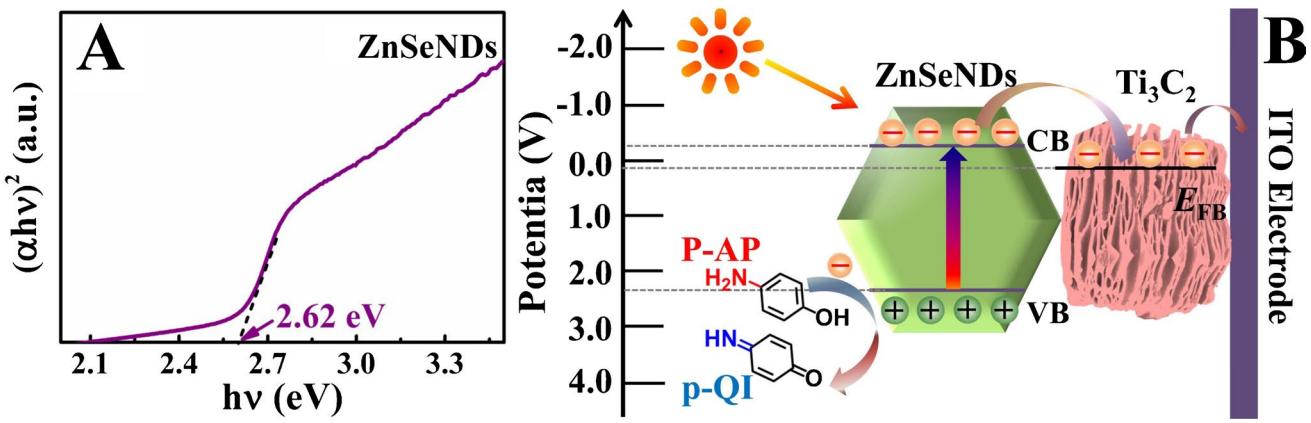

Fig. 3 **A** Tauc Plots, $(ahv)^2$ vs. hv, of ZnSeNDs; **B** Mechanism of ZnSeNDs:Ti_3C_2 photocathode under visible light. The potential vs Ag/AgCl

Table 1 Determination of ctDNA-KARS G12D in human serum samples ($n=5$) using the biosensor

Sample[a]	Original	Added (pM)	Found (pM)	qRT-PCR (pM)	RSD (%)	Recovery (%)
1	0.00	0.00	0.00	0.00	–	–
2	0.00	0.10	0.096	0.094	4.0	96.00
3	0.00	1.00	0.996	0.995	0.4	99.60
4	0.00	10.00	10.11	10.09	1.1	101.10
5	0.00	100.00	102.36	102.47	2.7	102.36

[a]The serum samples of healthy people were diluted tenfold with 10 mM PBS

double probes to the electrode surface via a Schiff base bond. Next, through strand displacement reaction, the recycling of the KARS G12D and the association of bio-FS strands on the sensor surface are realized at the same time. SA-ALP is captured through affinity between biotin and streptavidin. Benefiting from the high catalytic activity of ALP, *p*-APP can be catalyzed into *p*-AP in a short time, and the strong electron-donating ability of *p*-AP realizes the significant enhancement of PEC signal. In addition, PAGE consists with the results of photocurrent response and EIS (Fig. S3) to prove the successful construction of the dual amplification biosensor with AP oxidation amplification and KARS G12D cycling amplification.

Analytical performance of the ZnSeNDs:Ti_3C_2-based biosensor

The sensitivity of this method for the detection of KARS G12D was investigated under the optimum conditions. Figure S4A shows the relationship between the PEC response and the concentrations of the KARS G12D from 0.5 fM to 10 pM. It can be found that as the concentration of the KARS G12D increases, the PEC signal gradually increases. In addition, when the sensor concentration of the target is 0.5 to 100 fM, the logarithm of the signal is linear to the concentration. The regression equation is expressed as $I=0.903\ \log c+2.302$ ($R^2=0.9986$) (c, target concentration, fM). LOD is found to be 0.2 fM ($3S=N$. S, standard deviation; N, slope) ($n=9$). RSD is 3.4% at 2 fM. As the first PEC biosensor that uses ZnSeNDs:Ti_3C_2 as a photoactive material for biomarker detection, the biosensor based on toehold-mediated strand displacement reaction strategy has some advantages over previous reported method. As shown in Table S2, the biosensor achieves a wide linearity range and high sensitivity.

Specificity, stability, and reproducibility

Efficient differentiation of circulating tumor nucleic acid (ctNA) from its analogues is a vital factor to the sensor performance. The response of the sensor to different ctDNA was measured. Figure S5A shows the PEC responses of 10 pM EGFR, KIT^{L576P}, mir-196a, mir-196b, 1.0 pM KARS G12D, and their mixture, respectively. Only when the KARS G12D is present, the sensor shows obvious PEC signal enhancement, which fully demonstrates the specificity of the sensor. Then the stability was also measured. The PEC response is detected under successive periodic "off – on – off" light for five cycles, and the results are shown in Fig. S5B, and RSD of the photocurrent response signal is 3.6%. Reproducibility of five photoelectrode PEC assays was also done. The RSD is 4.1% ($n=5$) (Fig. S5C). These results indicate that the biosensor based on *p*-AP oxidation amplification and toehold-mediated strand displacement reaction has excellent specificity, stability, and reproducibility.

Analysis of human serum specimens

To evaluate the feasibility of this method, the KARS G12D in serum samples of healthy people were detected (S2). Samples spiked with KARS G12D (0.1 pM, 1.0 pM, 10.0 pM, and 100.0 pM) were included. As shown in Table 1, the recovery values ranging from 96.00 to 102.36% with an RSD of 0.4–2.7% are achieved ($n=5$), suggesting that this biosensor has potential for monitoring ctDNAs in complex biological samples. The concentrations of target were also detected with qRT-PCR. This shows no obvious difference between qRT-PCR and this biosensor.

Conclusion

In summary, a PEC method based on ZnSeNDs:Ti_3C_2 and non-enzyme toehold-mediated strand displacement reaction strategy to detect biomarker was build. After characterizing by SEM, TEM, XRD, electrochemical, and optical technology, the ZnSeNDs:Ti_3C_2 composite materials with excellent photoelectric performance were utilized to construct a PEC biosensor with signal amplification function of *p*-AP for the detection of KRAS G12D for the first time. The experimental results demonstrated that ZnSeNDs:Ti_3C_2-based biosensor showed excellent analytical performance for KRAS G12D detection and achieved a detection limit of 0.5

fM, proving that new composite materials based on MXene have a broad application prospect in biosensor construction.

Supplementary Information The online version contains supplementary material available at https://doi.org/10.1007/s00604-021-05117-0.

Funding This work was supported by the National Natural Science Foundation of China (21575073) and Laoshan Scholar Program of Qingdao University of Science and Technology (201802685).

Declarations

Conflict of Interest The authors declare no competing interests.

References

1. Wang H, Wu Y, Yuan X, Zeng G, Zhou J, Wang X, Chew JW (2018) Clay-inspired Mxene-based electrochemical devices and photo-electrocatalyst: state-of-the-art progresses and challenges. Adv Mater 30(12):1704561
2. Agresti A, Pazniak A, Pescetelli S, Di Vito A, Rossi D, Pecchia A, Auf der Maur M, Liedl A, Larciprete R, Kuznetsov DV, Saranin D, Di Carlo A (2019) Titanium-carbide Mxenes for work function and interface engineering in perovskite solar cells. Nat Mater 18(11):1228–1234
3. Huang K, Li C, Li H, Ren G, Wang L, Wang W, Meng X (2020) Photocatalytic applications of two-dimensional Ti_3C_2 Mxenes: a review. ACS Applied Nano Materials 3(10):9581–9603
4. Ding M, Xiao R, Zhao C, Bukhvalov D, Chen Z, Xu H, Tang H, Xu J, Yang X (2021) Evidencing interfacial charge transfer in 2d Cds/2d Mxene Schottky heterojunctions toward high-efficiency photocatalytic hydrogen production. Solar RRL 5(2):2000414
5. Cui C, Cheng R, Zhang H, Zhang C, Ma Y, Shi C, Fan B, Wang H, Wang X (2020) Ultrastable Mxene@Pt/Swcnts' nanocatalysts for hydrogen evolution reaction. Adv Func Mater 30(47):2000693
6. Yang Q, Huang Z, Li X, Liu Z, Li H, Liang G, Wang D, Huang Q, Zhang S, Chen S, Zhi C (2019) A Wholly Degradable, Rechargeable Zn–Ti_3C_2 Mxene capacitor with superior anti-self-discharge function. ACS Nano 13(7):8275–8283
7. Wang K, Zhou Y, Xu W, Huang D, Wang Z, Hong M (2016) Fabrication and thermal stability of two-dimensional carbide Ti_3C_2 nanosheets. Ceram Int 42(7):8419–8424
8. Nguyen V-H, Nguyen B-S, Hu C, Nguyen CC, Nguyen DL, Nguyen Dinh MT, Vo D-VN, Trinh QT, Shokouhimehr M, Hasani A, Kim SY, Le QV (2020) Novel architecture titanium carbide (Ti_3C_2Tx) Mxene cocatalysts toward photocatalytic hydrogen production: amini-review. Nanomaterials 10(4):602
9. Soomro RA, Jawaid S, Kalawar NH, Tunesi M, Karakuş S, Kilislioğlu A, Willander M (2020) In-situ engineered TiO_2/$BiVO_4$ hybrid as an efficient photoelectrochemical platform for sensitive detection of soluble CD44 proteins. Biosens Bioelectron 166:112439
10. Ishii K, Amagasu R, Nomura I (2019) Investigation of the N-side structures of II-VI compound semiconductor optical devices on Inp substrates. J Cryst Growth 512:96–99
11. Xia F, Shao Z, He Y, Wang R, Wu X, Jiang T, Duhm S, Zhao J, Lee S-T, Jie J (2016) Surface charge transfer doping via transition metal oxides for efficient *p*-type doping of II–VI nanostructures. ACS Nano 10(11):10283–10293
12. Ehsan MF, Shafiq M, Hamid S, Shafiee A, Usman M, Khan I, Ashiq MN, Arfan M (2020) Reactive oxygen species: new insights into photocatalytic pollutant degradation over G-C_3N_4/Znse nanocomposite. Appl Surf Sci 532:147418
13. Li D, Hussain S, Wang Y, Huang C, Li P, Wang M, He T (2021) Znse/Cdse Z-scheme composites with Se vacancy for efficient photocatalytic CO_2 reduction. Appl Catal B: Environ 286:119887
14. Wu L, Wang Y, Zhu L, Liu Y, Wang T, Liu D, Song Y, Yang C (2020) Aptamer-Based Liquid Biopsy. ACS Appl Bio Mater 3(5):2743–2764
15. Koo KM, Trau M (2020) Direct enhanced detection of multiple circulating tumor DNA variants in unprocessed plasma by magnetic-assisted bioelectrocatalytic cycling. ACS Sensors 5(10):3217–3225
16. Kaczor-Urbanowicz KE, Wei F, Rao SL, Kim J, Shin H, Cheng J, Tu M, Wong DTW, Kim Y (2019) Clinical validity of saliva and novel technology for cancer detection. Biochimica et Biophysica Acta (BBA) - Reviews on Cancer 1872(1):49–59
17. Huerta M, Roselló S, Sabater L, Ferrer A, Tarazona N, Roda D, Gambardella V, Alfaro-Cervelló C, Garcés-Albir M, Cervantes A, Ibarrola-Villava M (2021) Circulating tumor DNA detection by digital-droplet Pcr in pancreatic ductal adenocarcinoma: a systematic review. Cancers 13(5):994
18. Chen M, Wu D, Tu S, Yang C, Chen D, Xu Y (2021) CRISPR/Cas9 cleavage triggered Esdr for circulating tumor DNA detection based on a 3d graphene/Auptpd nanoflower biosensor. Biosens Bioelectron 173:112821
19. Zhang N, Shi X-M, Guo H-Q, Zhao X-Z, Zhao W-W, Xu J-J, Chen H-Y (2018) Gold nanoparticle couples with entropy-driven toehold-mediated DNA strand displacement reaction on magnetic beads: toward ultrasensitive energy-transfer-based photoelectrochemical detection of Mirna-141 in real blood sample. Anal Chem 90(20):11892–11898
20. Tahir R, Renuse S, Udainiya S, Madugundu AK, Cutler JA, Nirujogi RS, Na CH, Xu Y, Wu X, Pandey A (2021) Mutation-specific and common phosphotyrosine signatures of Kras G12d and G13d alleles. J Proteome Res 20(1):670–683
21. Kargbo RB (2021) Targeting the Kras G12d mutant as potential therapy in cancer. ACS Med Chem Lett 12(8):1212–1213
22. Zhu W, Hutchison JA, Dong M, Li M (2021) Frequency shift surface-enhanced raman spectroscopy sensing: an ultrasensitive multiplex assay for biomarkers in human health. ACS Sensors 6(5):1704–1716
23. Lin J, Yu Y, Zhang Z, Gao F, Liu S, Wang W, Li G (2020) A novel approach for achieving high-efficiency photoelectrochemical water oxidation in Ingan nanorods grown on Si system: Mxene nanosheets as multifunctional interfacial modifier. Adv Func Mater 30(13):1910479
24. Shi Z, Liu J, Liu D, Zhang Q, Lang J, Li X (2019) Preparation and comparison of the photocatalytic properties of Znse with different crystalline phases. Physica status solidi (b) 256(8):1800754
25. Bian X, Guo B, Zhao M, Han D, Cheng W, Song F, Ding S (2019) An Enzyme-free "on-off" electrochemiluminescence biosensor for ultrasensitive detection of Pml/Rarα based on target-switched DNA nanotweezer. ACS Appl Mater Interfaces 11(4):3715–3721
26. Singh N, Rai P, Ali MA, Kumar R, Sharma A, Malhotra BD, John R (2019) A Hollow-nanosphere-based microfluidic biosensor for biomonitoring of cardiac troponin I. J Mater Chem B 7(24):3826–3839
27. Ran J, Gao G, Li F-T, Ma T-Y, Du A, Qiao S-Z (2017) Ti_3C_2 Mxene co-catalyst on metal sulfide photo-absorbers for enhanced visible-light photocatalytic hydrogen production. Nat Commun 8:13907–13907
28. Li M, Wang H, Wang X, Lu Q, Li H, Zhang Y, Yao S (2019) Ti_3C_2/Cu_2O Heterostructure based signal-off photoelectrochemical sensor for high sensitivity detection of glucose. Biosens Bioelectron 142:111535

29. Alhabeb M, Maleski K, Mathis TS, Sarycheva A, Hatter CB, Uzun S, Levitt A, Gogotsi Y (2018) Selective etching of silicon from Ti_3SiC_2 (MAX) to obtain 2d titanium carbide (Mxene). Angew Chem Int Ed 57(19):5444–5448
30. Ge XL, Di HX, Wang P, Miao XG, Zhang P, Wang HY, Ma JY, Yin LW (2020) Metal-organic framework-derived nitrogen-doped cobalt nanocluster inlaid porous carbon as high-efficiency catalyst for advanced potassium-sulfur batteries. ACS Nano 14(11):16022–16035
31. Sun Y, Zhang YM, Zhang HX, Liu ML, Liu Y (2020) Integrating highly efficient recognition and signal transition of G-C_3N_4 embellished Ti_3C_2 Mxene hybrid nanosheets for electrogenerated chemiluminescence analysis of protein kinase activity. Anal Chem 92(15):10668–10676
32. Ikram A, Dass S, Shrivastav R, Satsangi VR (2019) Integrating Pbs quantum dots with hematite for efficient photoelectrochemical hydrogen production. Physica status solidi (a) 216(7):1800839
33. Han S-Y, Pan D-L, Chen H, Bu X-B, Gao Y-X, Gao H, Tian Y, Li G-S, Wang G, Cao S-L, Wan C-Q, Guo G-CA (2018) A methylthio-functionalized-MOF photocatalyst with high performance for visible-light-driven H_2 evolution. Angewandte Chemie (International ed. in English) 57(31):9864–9869
34. Hile DD, Swart HC, Motloung SV, Motaung TE, Koao LF (2019) Structural, morphological and optical studies of zinc selenide (Znse) thin films synthesized at different deposition time intervals using photo-assisted chemical bath deposition technique. Physica B: Condensed Matter 575:411706
35. Wang L, Tian G, Chen Y, Xiao Y, Fu H (2016) In situ formation of a Zno/Znse nanonail array as a photoelectrode for enhanced photoelectrochemical water oxidation performance. Nanoscale 8(17):9366–9375
36. Mendonça CD, Rahemi V, Hereijgers J, Breugelmans T, Machado SAS, De Wael K (2020) Integration of a photoelectrochemical cell in a flow system for quantification of 4-aminophenol with titanium dioxide. Electrochem Commun 117:106767
37. Wang J, Zhang H, Zhao J, Zhang R, Zhao N, Ren H, Li Y (2019) Simultaneous determination of paracetamol and *p*-aminophenol using glassy carbon electrode modified with nitrogen- and sulfur-co-doped carbon dots. Microchim Acta 186(11):733
38. Kumbhar D, Kumbhar S, Salunke G, Nalawade R, Nalawade A (2019) Effect of Cu doping on structural and optical properties of Zno nanoparticles using sol–gel method. Macromol Symp 387(1):1800192
39. Romani L, Speltini A, Ambrosio F, Mosconi E, Profumo A, Marelli M, Margadonna S, Milella A, Fracassi F, Listorti A, De Angelis F, Malavasi L (2021) Water-stable $DMASnBr_3$ lead-free perovskite for effective solar-driven photocatalysis. Angew Chem Int Ed 60(7):3611–3618
40. Wang Q, Yu S, Qin W, Wu X (2020) Isopropanol-assisted synthesis of highly stable $MAPbBr_3$/*p*-g-C_3N_4 intergrowth composite photocatalysts and their interfacial charge carrier dynamics. Nanoscale Advances 2(1):274–285
41. Zhu J, Bošković F, Nguyen B-NT, Nitschke JR, Keyser UF (2021) Kinetics of toehold-mediated DNA strand displacement depend on $Fe^{II}_4L_4$ tetrahedron concentration. Nano Lett 21(3):1368–1374
42. Luo T, Fan S, Liu Y, Song J (2021) Information processing based on DNA toehold-mediated strand displacement (TMSD) reaction. Nanoscale 13(4):2100–2112
43. Li J, Yang F, Jiang B, Zhou W, Xiang Y, Yuan R (2020) The synchronization of multiple signal amplifications for label-free and sensitive aptamer-based sensing of a protein biomarker. Analyst 145(24):7858–7863
44. Irmisch P, Ouldridge TE, Seidel R (2020) Modeling DNA-strand displacement reactions in the presence of base-pair mismatches. J Am Chem Soc 142(26):11451–11463
45. Rodríguez-Serrano AF, Hsing IM (2021) Allosteric regulation of DNA circuits enables minimal and rapid biosensors of small molecules. ACS Synth Biol 10(2):371–378